ISSN 1330–0016
CODEN FIZBE7

STUDY OF H $\to$ ZZ $\to 4\ell^{\pm}$ WITH A FULL GEANT SIMULATION OF CMS DETECTOR

DEANA BOMEŠTAR[a], DANIEL DENEGRI[b], RITVA KINNUNEN[c] and ALEXANDRE NIKITENKO[d]

[a] *Institute Ruđer Bošković, Zagreb, Croatia*
[b] *DAPNIA/ SPP,CEN Saclay, France*
[c] *SEFT, University of Helsinki, Finland*
[d] *ITEP, Moscow, Russia*

Dedicated to Professor Mladen Paić on the occasion of his 90$^{\text{th}}$ birthday

Received 11 July 1995

UDC 539.12

PACS 06.90.+v

We study the detection of H $\to$ ZZ $\to 4\ell^{\pm}$ in the CMS detector at the nominal LHC energy $\sqrt{s} = 14$ TeV and the possibility for an early detection at a reduced energy $\sqrt{s} = 10$ TeV. A systematic study of the multi–lepton mass resolution is performed, including effects of internal and external radiation through detailed GEANT simulations. At $\sqrt{s} = 14$ TeV, an integrated luminosity of 10^4 pb^{-1} allows exploration at a $\geq 5\sigma$ significance level a mass range from $m_H \approx 2m_Z$ up to $m_H \approx$ 400 GeV. For 10^5 pb^{-1}, the mass reach is about 650 GeV. At $\sqrt{s} = 10$ TeV, an integrated luminosity of 10^4 pb^{-1} does not provide a 5σ significance level for any value of Higgs mass, and 2×10^4 pb^{-1} alows one to explore a mass range from $m_H \approx 2m_Z$ to ≈ 350 GeV at $\geq 5\sigma$ level.

1. Introduction

The future Large Hadron Collider (LHC) at CERN is designed to bring protons into head-on colissions at an energy of 14 TeV in the center–of–mass frame and

with a luminosity from 10^{33} cm^{-2}s^{-1} to 10^{34} cm^{-2}s^{-1}. Two huge general purpose detectors are foreseen, CMS (Compact Muon Solenoid) and ATLAS (A Toroidal LHC Apparatus). They are optimized for the search of the Higgs boson over a mass range from about 90 GeV to about 1 TeV, but they also allow detection of a wide range of possible signatures from alternative electro–weak symmetry breaking mechanisms [1].

The most convenient channel to search for Standard Model (SM) Higgs is H → ZZ → 4$\ell^{\pm}$ (ℓ =e, μ), due to the relatively large cross–section and simple signature. The signal appears as a Breit-Wigner peak in a four-lepton invariant mass distribution over a continuum ZZ background. This channel allows an early search of the SM Higgs boson over a significant mass range (from $2m_Z$ threshold upwards), already in the $L \approx 10^{33}$ cm^{-2}s^{-1} luminosity regime of the LHC. Detection of the Higgs in this channel relies on good lepton acceptance and on precise reconstruction of the two Z's in the event.

The main background in this channel arises from SM continuum ZZ production. Because of the presence of the two real Z's, this background is difficult to reduce. The $t\bar{t}$ background is small. With $m_{top} = 174$ GeV, it is only a minor contribution in the $m_H \approx 200$ GeV range. At $m_H = 200$ GeV, the natural width of the Higgs is still small, $\Gamma_H = 1.5$ GeV, and a good four lepton mass resolution would clearly ease an early observation of the signal in the $m_H \leq 300$ GeV region where the cross–section is largest. However, the external brehmsstrahlung loss in the material of the tracker degrades Z and Higgs mass resolution, resulting in a significant loss of events. Full GEANT simulations are performed to reconstruct the H → ZZ → 4$e^{\pm}$ events in the crystal calorimeter, allowing partial recovery of the radiation losses [8].

Here we study the detection of the H → ZZ → 4$\ell^{\pm}$ signal in CMS detector at the nominal LHC energy $\sqrt{s} = 14$ TeV and the early detection capability at LHC with a reduced cms energy of 10 TeV.

2. The model

2.1. Signal and background simulation

Events are generated by PYTHIA 5.7 with CTEQ2L structure functions [2]. The top quark mass is set to 174 GeV, according to the recent CDF result [3]. The production processes included are: gg fusion ($gg \to$ H), the WW and ZZ fusion (WW → H and ZZ → H), and the $q\bar{q} \to$ H process, where the Higgs is produced in association with heavy flavours, the latter one contributing only about 3% to the total cross–section for $m_H = 200$ GeV, and less than 1% for masses greater than $m_H = 300$ GeV. The main contribution comes from gg fusion and amounts to about 70% of the total rate for $m_H = 200$ GeV. For $m_{top} = 174$ GeV, the relative contribution of gg fusion is largest for $m_H = 400$ GeV (about 80%), and decreases towards higher masses, being about 70% for $m_H = 600$ GeV. The cross–section times branching ratio ($\sigma \cdot BR$) for H → ZZ → 4$\ell^{\pm}$ for Higgs masses from 190 to

600 GeV is given in Table 1. The contributions from $q\bar{q}, gg$ and WW/ZZ fusion are shown separately.

TABLE 1.
$\sigma \cdot BR$ for $H \to ZZ \to 4\ell^{\pm}$ *and* ZZ*–background at LHC energy 14* TeV.

m_H [GeV]	190	200	250	300	350	400	500	600	ZZ
$\sigma_{t\bar{t}}$ [fb$\times 10^{-2}$]	30.9	31.5	16.6	8.3	4.3	2.2	1.2	0.5	
σ_{gg} [fb]	6.99	8.23	7.09	6.06	6.21	5.22	2.50	1.15	
$\sigma_{WW/ZZ}$ [fb]	2.84	3.15	2.79	2.21	1.73	1.25	0.72	0.47	
σ_{total} [fb]	10.14	11.69	10.05	8.35	7.98	6.49	3.23	1.63	59.6

The main background in this channel is non–resonant ZZ production, and is largely irreducible. Only the $q\bar{q} \to ZZ$ subprocess is simulated in PYTHIA. To estimate $gg \to ZZ$ contribution, we have used the calculation of Ref. 4. Similar event topology and kinematics in these two processes allows one to incorporate (approximately) the gg contribution by multiplying the $q\bar{q} \to ZZ$ cross–section by a factor of 1.33, adequate for the m_H range investigated here. The total cross–section for continuum $ZZ \to 4\ell^{\pm}$ is given also in Table 1. No k-factors are included, neither for the signal nor for the background.

High p_T electrons and muons radiate photons due to QED bremsstrahlung. To generate internal bremsstrahlung photon emission, a dedicated photon radiation program PHOTOS 2.0 [5] is used. The fraction of events falling outside the $m_Z \pm 6$ GeV window due to internal bremsstrahlung is 7% for $Z \to \mu^+\mu^-$ and 12% for $Z \to e^+e^-$, prior to any detector response simulation effect was included.

2.2. Detector simulation

The heart of the CMS detector is a long (13 m) superconducting solenoid with a 6 m diameter bore and a uniform 4 T field, containing the inner tracker surrounded with electromagnetic (ECAL) and hadronic (HCAL) calorimeters. The magnetic flux is returned through a 2 m thick iron yoke (with a 1.8 T return field) instrumented with four layers of muon chambers. The high–granularity ECAL is made of high–resolution $PbWO_4$ crystals (about 10^5 crystals), ensuring precise measurement of electrons and photons. Central tracker and ECAL cover a region $|\eta| \leq 3$. To ensure hermeticity and for measuring forward "tagging" jets, there is in addition a very forward calorimeter extending up to $|\eta| = 5$.

The electron and muon momentum resolutions have been studied using detailed GEANT simulations of detector response, including beam pipe, active and passive detector volumes and materials, support structure, cooling, electronics and the track reconstruction procedure [6, 7]. The resulting muon resolution ($\Delta p/p < 1.4\%$ for $p_T^{\mu} < 100$ GeV) is parametrized as a function of p and η and is used here to smear the momenta of the muons. The momentum measurement of electrons is significantly degraded by bremsstrahlung in the material of the tracker. The external bremsstrahlung loss on electron energy depends on the amount of material

traversed and hence on the electron rapidity. This effect is sizable for the present CMS tracker design, having on average 27% of radiation length before the last measuring layer in the tracker. Thus measuring the electron energy in the electromagnetic calorimeter, rather than the momentum in the tracker leads to a better multi–electron mass resolution and efficiency, if the size of the crystal matrix around the electron impact point is chosen such that it contains a substantial fraction of the bremsstrahlung photons. Full GEANT simulations of the channels $H \to ZZ \to 4e^{\pm}$ and $H \to ZZ^* \to 4e^{\pm}$ have been carried out to optimize the size of the matrix used to measure the electron or positron energy [8]. As the magnetic field deflects the electron from the radiated photons in the ϕ direction, the size of the matrix is larger in ϕ than in η and asymmetrical, depending on the particle charge. For crystals of lateral size 1.8 cm × 2.1 cm, i.e $\Delta\eta \times \Delta\phi = 0.013 \times 0.016$, a 5(in η)×7(in ϕ) crystal matrix seems at present to be a good choice for the reconstruction of the Z and Higgs boson masses. Further work is needed to define more sophisticated algorithms to recover still larger fraction of electrons, but here we use this simple 5×7 matrix algorithm.

In conclusion, the $Z \to \ell^+\ell^-$ from the $H \to ZZ \to 4\ell^{\pm}$ and $H \to 4\ell^{\pm}$ mass reconstruction, resolution and reconstruction efficiency for different values of m_H, have been studied with detailed GEANT simulations [6 – 8], and resulting efficiencies and resolutions again parametrized for faster simulations where appropriate, but where radiative effects are essential, it is the direct GEANT simulation which is used in the following.

In order to account for additional trigger and geometrical inefficiences (fiducial volume loss), an additional reconstruction efficiency per lepton of 0.95 for both electrons and muons is used. We think that such a reconstruction efficiency is achievable in the $ZZ \to 4\ell^{\pm}$ final state, as, despite a 10% fiducial volume loss for a purely calorimetric electron measurement, this can be complemented by the tracker measurement, and similarly for a hard and isolated muon not recognized in muon chambers.

2.3. Signal selection

Events are required to have four leptons with:

i) one electron with $E_T > 20$ GeV, one with $E_T > 15$ GeV, and the remaining two electrons with $E_T > 10$ GeV, all within $|\eta| < 2.5$. For muons, the corresponding p_T cuts are 20, 10 and 5 GeV, all in the rapidity range $|\eta| < 2.4$. The event can comprise a pair of muons and a pair of electrons. At $m_H = 200$ GeV (600 GeV) the average signal acceptance for these cuts, summed over $4e^{\pm}$, $4\mu^{\pm}$ and $2e^{\pm}2\mu^{\pm}$ modes, is 59% (78%) and for the ZZ background it is 44%.

ii) Two lepton (e^+e^- or $\mu^+\mu^-$) pairs with an invariant mass consistent with a Z mass are required. The Z mass window we use is $m_Z \pm 6$ GeV, what corresponds to about $\pm 3\sigma_Z$ around m_Z.

No lepton isolation cuts are applied, because there is no background whose reduction is critically dependent on isolation; in the whole mass range, ZZ con-

tinuum is the dominant background and the $t\bar{t}$ is only a minor contribution (with $m_{top} = 174$ GeV) in the $m_H \approx 200$ GeV range.

3. Z mass resolution

Figure 1 shows a) Z → e^+e^- from H → 4$e^{\pm}$ and b) Z → $\mu^+\mu^-$ from H → 4$\mu^{\pm}$ mass distributions at $m_H = 300$ GeV, including all radiative losses and instrumental effects. In the electron channel, the Z mass is reconstructed with full GEANT simulations [8]. In simulations, we introduce an energy equivalent of noise of 50 GeV per crystal, and a smearing of the cluster energy by $5\%/\sqrt{E}$ stochastic (for photostatistic) and a 0.5% constant term. Due to the external bremsstrahlung, Z and Higgs mass resolutions in the electron channel are worse than those in the muon channel. The resolution for Z → e^+e^-, obtained from a Gaussian fit to the peak region, is 2.1 GeV. The Z mass resolution, σ_Z, in the muon channel is 1.8 GeV. In the following, we make a systematic study of the separate contributions to the mass resolution of the natural width, momentum resolution and of the effects of radiative losses.

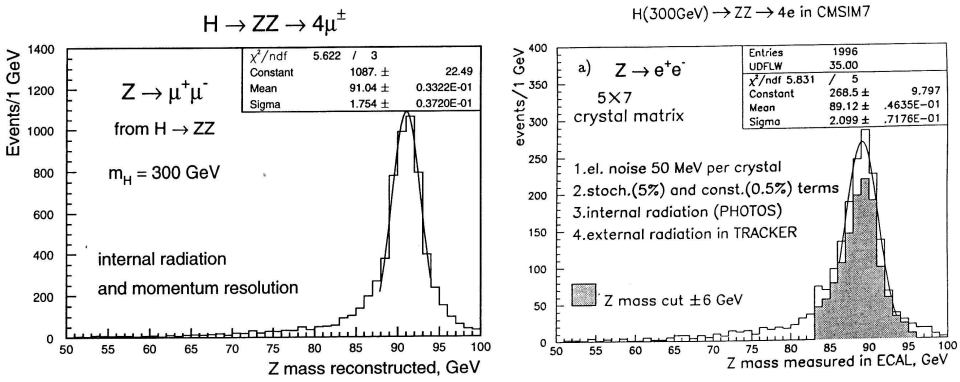

Fig. 1. a) Z → e^+e^- mass reconstructed from the H → ZZ → 4$e^{\pm}$ *decays for* $m_H = 300$ GeV *including internal and external radiation and energy resolution. b) Z → $\mu^+\mu^-$ mass reconstructed from the* H → ZZ → 4$\mu^{\pm}$ *decays for* $m_H = 300$ GeV, *including internal radiation and momentum resolution.*

We recall that the multi–lepton mass resolution is affected, on top of the possible effect of the natural width of Z and H, in the muon channel by internal radiation and momentum resolution, and in the electron channel by internal and external radiation in the tracker and by the energy resolution in the ECAL.

The results of a systematic study of Z mass resolution in Z → $\mu^+\mu^-$ for Higgs masses from 120 GeV to 800 GeV are shown in Fig. 2. Three cases are considered: a) pure (BW) signal, with no radiation and no instrumental effects, b) with internal bremsstrahlung and c) with both internal bremsstrahlung and momentum resolution. The Z natural width corresponds in this Gaussian fit to $\sigma_Z \approx 1.3$ GeV in the chosen mass range, and it is independent of m_H. The effect of internal

bremsstrahlung is small, increasing σ_Z to about 1.4 GeV over the whole investigated Higgs mass range. If we include also momentum resolution effects, for $m_H < 300$ GeV, the Z mass resolution ($\sigma_Z < 1.8$ GeV) is still dominated by the contribution from the Z natural width, i.e. it is not much affected by the momentum resolution. With increasing Higgs mass, and thus the Z boost, however, the muon momentum resolution becomes the dominant effect, σ_Z increasing with Higgs mass from $\sigma_Z \approx 1.8$ GeV at $m_H = 300$ GeV to $\sigma_Z \approx 2.5$ GeV at $m_H = 800$ GeV.

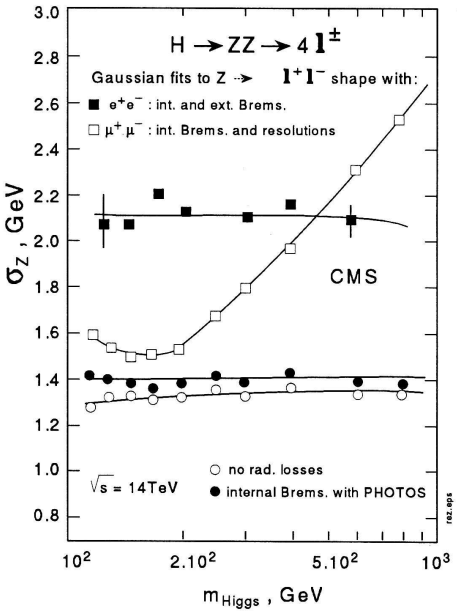

Fig. 2. $Z \to \mu^+\mu^-$ *and* $Z \to e^+e^-$ *(from the* $H \to ZZ \to 4\mu^{\pm}, 4e^{\pm}$ *decays) mass resolutions for* $m_H = 120$ *to 800* GeV *obtained from fits to the Gaussian part of the mass distributions.*

The $Z \to e^+e^-$ mass resolutions obtained with the detailed GEANT simulations of electron behaviour in tracker and ECAL are also shown in Fig. 2. The external bremsstrahlung losses are partly recovered by measuring electron energies in the crystal calorimeter, insuring better efficiency; the Z mass resolution in the electron channel does not vary significantly with Higgs mass and is about 2.1 GeV on average. It does not improve with increasing m_H or $Z \to e^+e^-$ boost, as it is dominated by the $e^{\pm}$ reconstruction algorithm (improvements are still possible in the future).

3.1. Z *reconstruction efficiency and efficiency of* Z *mass cut*

For Higgs masses $m_H \geq 2m_Z$, the Z mass window we use to reconstruct Higgs mass is large, $m_Z \pm 6$ GeV, since there are no backgrounds that need or can be suppressed by the two–lepton mass cut. Due to bremsstrahlung and momentum

resolution, the typical Z reconstruction efficiency in this mass range is about 80% in both muon and electron channels. In the signal selection, two e^+e^- or $\mu^+\mu^-$ pairs with an invariant mass consistent with a Z mass are required, thus 36% to 38% of the events are rejected by the two–lepton mass cut. No attempt is done yet to recover part of large-angle bremsstrahlung losses.

4. Higgs mass resolution

Good 4-lepton mass resolution is of great importance in the H → ZZ* → 4$\ell^{\pm}$ channel, where the natural width of the Higgs boson is very small. Figure 3 shows a) the H → 4$\mu^{\pm}$ and b) the H → 4e$^{\pm}$ mass distribution for $m_H = 150$ GeV. In the figures are only those events which satisfy the condition $|m_Z - m_{\mu\mu}| \leq 3\sigma_Z$ (3a) or $|m_Z - m_{ee}| \leq 3\sigma_Z$ (Fig. 3b). All radiation losses and instrumental effects are included. Radiation by the electrons from the Z* is responsible for the large low-mass radiative tail in the H → 4e$^{\pm}$ distribution.

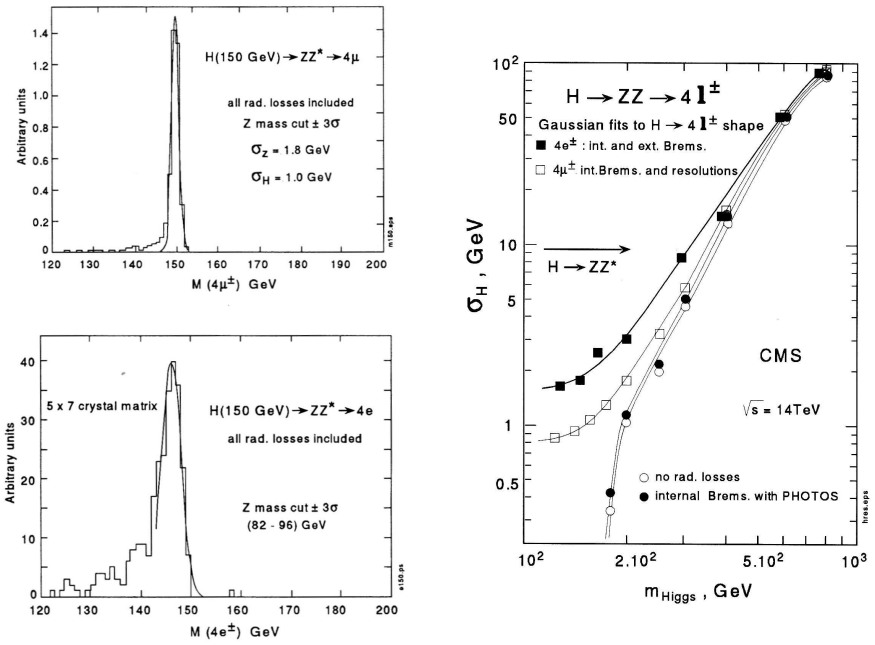

Fig. 3. a) H → 4$\mu^{\pm}$ *mass distribution for* $m_H = 150$ GeV. *Internal radiation, momentum resolution and* Z *reconstruction efficiency are included.*
b) H → 4e$^{\pm}$ *mass distribution for* $m_H = 150$ GeV. *Internal and external radiation, energy resolution in ECAL and efficiency of the* Z *mass cut are included.*

Fig. 4. H → 4$\mu^{\pm}$ *and* H → 4e$^{\pm}$ *mass resolutions for* $m_H = 130$ *to 800* GeV, *obtained from fits to the Gaussian part of the mass distributions after the* Z *mass cut is imposed (right).*

Figure 4 shows the H → ZZ → 4 $\mu^{\pm}$ mass resolution versus m_H after the Z mass cut is imposed, for each of three cases discussed in the Section 3. The H → ZZ → 4e$^{\pm}$ mass resolution from ECAL measurements, including all radiation losses [8], is also given. In the low mass range, $m_H < 200$ GeV, where the 4-lepton mass resolution plays a crucial role to extract the H → ZZ* signal, the resolutions are $\sigma^H_{4\mu} \approx 1$ GeV and $\sigma^H_{4e} \approx 2$ GeV and are entirely dominated by the momentum resolution for muons and by radiation losses for electrons, as the natural width of the Higgs boson is very small (e.g., the natural width of the Higgs boson is 19 MeV at $m_H = 150$ GeV). For Higgs masses beyond 300 GeV, the natural width of the Higgs boson dominates the four–lepton mass resolution.

5. *Signal significance at the nominal LHC cms energy of 14* TeV.

We now address the issue of H → ZZ → 4$\ell^{\pm}$ signal significance at the nominal LHC energy $\sqrt{s} = 14$ TeV in the Higgs mass range from $2m_Z$ upwards, taking

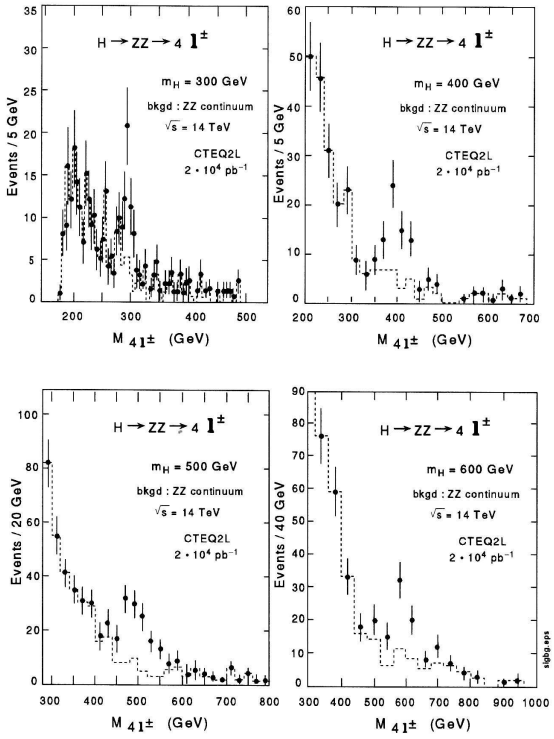

Fig. 5. Four-lepton mass distributions for the H → ZZ → 4$\ell^{\pm}$ *signal superimposed on the* ZZ *continuum background for different values of* m_H.

into account all radiation losses and instrumental effects, and the efficiency of the selection cuts (lepton p_t, rapidity, Z mass cut). In that case, the efficiency for reconstructing H → ZZ → 4$\ell^{\pm}$ varies from about 30% at $m_H = 200$ GeV to about 41% at $m_H = 600$ GeV, and is 23% for ZZ background. The specific signal selection and background suppression criteria for the $m_H < 2m_Z$ region are not the subject of this study. They are discussed in great detail in Ref. 9.

Figure 5 shows the single experiment simulation of the expected four-lepton mass distributions for the H → ZZ → 4$\ell^{\pm}$ signal, superimposed on the ZZ continuum background, for $m_H = 300$ GeV and an integrated luminosity 2×10^4 pb^{-1}, and for m_H =300, 500 and 600 GeV with 10^5 pb^{-1}. For $m_H = 300$ GeV, where electron radiative effects are still significant, the electron spectrum from full GEANT simulation is incorporated for electron final states.

TABLE 2.

The mean value and Gaussian sigma for the combined 4-lepton mass distribution from H → ZZ → 4$\ell^{\pm}$. *The following two rows show the final number of events for the Higgs signal and for the* ZZ *background in the* $m_{4l} \pm 2\sigma_{4l}$ *window, calculated with the CTEQ2L structure functions at LHC energy 14* TeV *and with* 10^4 pb^{-1}. *The resulting significances given in the last row are calculated according to Poisson statistics.*

m_H [GeV]	190	200	250	300	350	400	500	600
m_{4l} [GeV]	189.1	198.7	248.0	298.1	347.9	395.4	490	579
σ_{4l} [GeV]	1.8	2.3	4.4	7.0	10.5	16.0	31	53
N_S	23.3	27.5	23.5	21.4	21.1	18.6	10.2	5.3
N_B	8.9	12.6	12.3	10.4	8.4	7.8	6.4	5.7
Significance	5.9	6.1	5.2	5.1	5.5	5.1	3.1	1.9

Table 2 gives the expected number of events with 10^4 pb^{-1} for the H → ZZ → 4$\ell^{\pm}$ signal and for the ZZ background for several m_H values between 190 and 600 GeV, after selection cuts (lepton p_T threshold, rapidity, Z mass window), including internal and external bremsstrahlung and momentum resolution, and taking into account an additional lepton reconstruction efficiency of 95%. The 4-lepton mass is required to be within $\pm 2\sigma_{4l}$ around the reconstructed Higgs mass peak m_{4l}. The values of σ_{4l} and m_{4l}, shown also in the table, are obtained from Gaussian fits to the combined 4-lepton mass distributions to provide estimates of the widths and the peak position of the 4-lepton spectra. Mainly due to the external radiation losses, the peak position is shiffted and the reconstructed Higgs mass is smaller than m_H generated (e.g. for $m_H = 600$ GeV this shifft is about 20 GeV). For large masses, where the mass distribution is dominated by the natural width, a Gaussian description is clearly not adequate and further work is needed to develop a proper method.

Figure 6 shows the expected H → ZZ → 4$\ell^{\pm}$ signal significance (for signal within $\pm 2\sigma_{4l}$), calculated according to Poisson statistics, for several integrated luminosities ranging from 5×10^3 to 10^5 pb^{-1}. Significance in the H → ZZ* → 4$\ell^{\pm}$ channel with 10^5 pb^{-1} is also shown in Fig. 6 and is discussed in Ref. 9.

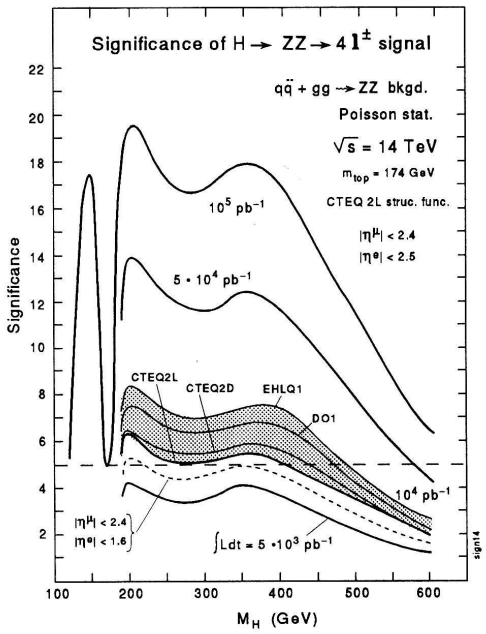

Fig. 6. Significance of the H → ZZ → 4$\ell^{\pm}$ *signal at* $\sqrt{s} = 14$ TeV *as a function of* m_H *for different luminosities. The band for* 10^4 pb^{-1} *represents the uncertainty in the signal significance related to structure functions. The dashed line represents the signal significance (CTEQ2L structure functions,* 10^4 pb^{-1}*) with a detector acceptance for electrons limited to the barrel region* $|\eta| < 1.6$.

Already with 10^4 pb^{-1}, the discovery region at the 5σ significance level extends from $m_H \approx 180$ GeV up to $m_H \approx 400$ GeV, and at the 3σ level up to $m_H \approx 500$ GeV. The significance is somewhat reduced around $m_H \approx 300$ GeV, due to the suppressed cross–section for $gg \to$ H for $m_{top} = 174$ GeV. With 10^5 pb^{-1}, the 5σ discovery range extends up to about 650 GeV, the exact upper reach depending on a more exact treatment of the BW shape of Higgs signal, and of interference effects with background.

The uncertainty in the signal significance related to structure functions is shown in Fig. 6 as a band for 10^4 pb^{-1}. The most recent sets, CTEQ2L and CTEQ2D, result in a reduced significance compared to the older sets DO1 and EHLQ1, due to the lower signal production cross-section.

5.1. Dependence on the electron rapidity coverage

In a possible staging scenario of the CMS detector, electrons would be detected with the crystal calorimeter limited to the barrel, i.e. $|\eta| < 1.6$ instead of $|\eta < 2.5|$. It is interesting to check how this reduced detector acceptance for electrons affects the signal significance. The reduction in the number of events for the combined 4-

lepton final state is on the average 27% for the signal and 34% for the background. Thus, the signal significance is reduced by 10%, and with 10^4 pb^{-1} it falls below the 5σ level for all masses above $m_H \approx 200$ GeV, as shown by the dashed line in Fig. 6.

6. *Signal significance at LHC cms energy of 10* TeV

Cross–sections ($\sigma \cdot BR$) for the $H \to ZZ \to 4\ell^{\pm}$ signal for Higgs masses between 190 and 600 GeV and for the ZZ continuum background are given in the Table 3. Contributions from gg and WW fusion are shown separately.

TABLE 3.
Cross–sections for signal and background at the reduced LHC energy 10 TeV*, the corressponding final number of events and signal significance within $\pm\sigma_{4l}$ around m_{4l} with $10^4\, pb^{-1}$*

m_H [GeV]	190	200	250	300	350	400	500	600	ZZ
σ_{gg} [fb]	4.1	4.5	3.8	3.1	3.1	2.5	1.1	0.5	
$\sigma_{WW/ZZ}$ [fb]	1.5	1.7	1.4	1.1	0.8	0.6	0.3	0.2	
σ_{total} [fb]	5.7	6.3	5.3	4.2	3.9	3.1	1.4	0.7	39.5
N_S	14.0	16.5	14.2	11.6	11.2	9.4	4.8	2.5	
N_B	6.8	9.4	9.2	7.7	5.8	5.9	4.5	3.8	
Significance	4.0	4.1	3.7	3.3	3.7	3.0	1.7	0.9	

At $\sqrt{s} = 10$ TeV, efficiency of lepton η and p_T cuts for signals increases from 66% at $m_H = 200$ GeV to 83% at $m_H = 600$ GeV, and it is 49% for background (summed over $4e^{\pm}$, $4\mu^{\pm}$ and $2e^{\pm}2\mu^{\pm}$ modes).

Figures 7a and 7b show signal cross–sections before and after p_T and $|\eta|$ acceptance cuts at $\sqrt{s} = 10$ TeV. For comparison, the values obtained at $\sqrt{s} = 14$ TeV are also shown. The fall of the production cross–section when $\sqrt{s}$ decreases from 14 to 10 TeV is fast, being 46% for $m_H = 200$ GeV, and increasing to 56% for $m_H = 600$ GeV (Fig.7a). Because the relative geometrical acceptance increases with decreasing $\sqrt{s}$, the decrease of the cross–section is smaller after the p_T and $|\eta|$ cuts are applied (40% for $m_H = 200$ GeV and 53% for $m_H = 600$ GeV) (Fig.1b). For the ZZ background, the cross–section within the η and p_T acceptance is only 26% lower at 10 TeV than that at 14 TeV.

Figures 8a and 8b show an example of the expected 4-lepton mass spectrum, with $m_H = 200$ and 400 GeV signal, superimposed on the expected ZZ background. As in the 10 TeV regime, the instantaneous luminosity is limited to $< 2 \times 10^{33}$ cm$^{-2}s^{-1}$, the event rates are calculated for 2×10^4pb^{-1}.

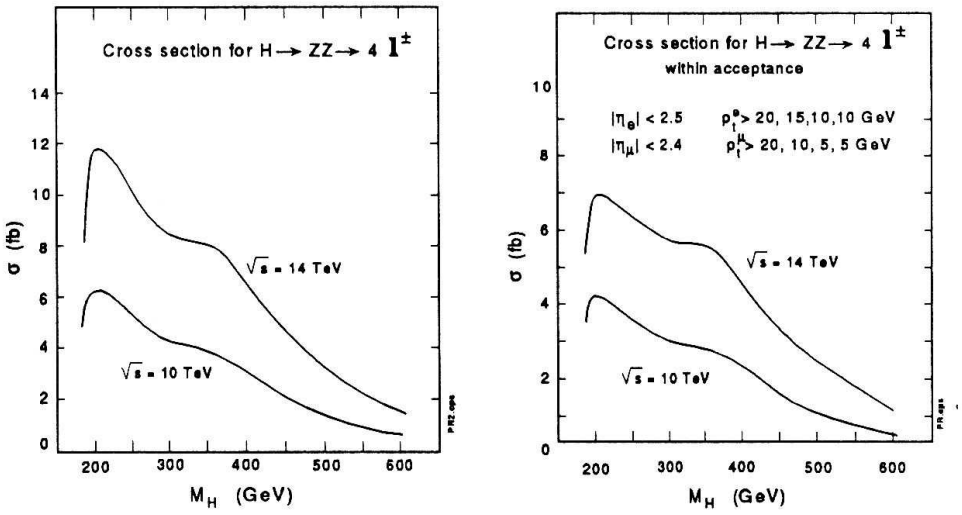

Fig. 7. $\sigma \cdot BR$ *for* $\mathrm{H} \to \mathrm{ZZ} \to 4\ell^{\pm}$ *versus* m_H *at* $\sqrt{s} = 10$ *and* 14 TeV *before and after lepton* η *and* p_T *cuts.*

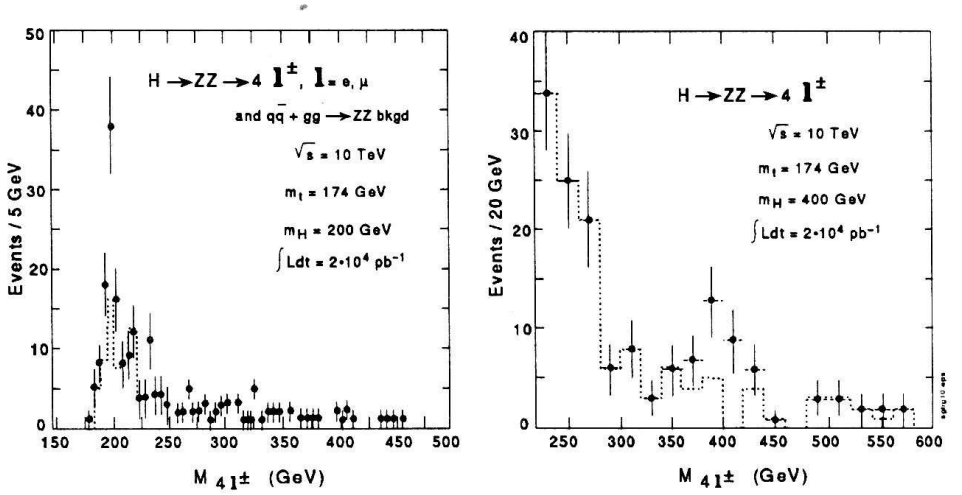

Fig. 8. The 4-lepton mass distribution for $\mathrm{H} \to \mathrm{ZZ} \to 4\ell^{\pm}$ *at* $m_H = 200$ GeV *and* $m_H = 400$ *GeV, superimposed on the ZZ continuum background (dashed line) at* $\sqrt{s} = 10$ TeV. *The even rates are calculated with* $2 \times 10^4 \mathrm{pb}^{-1}$.

Table 3 gives the expected number of events for signal and background for $\sqrt{s} =$ 10 TeV with $10^4 \mathrm{pb}^{-1}$, after the 4-lepton mass cut is imposed. All the radiative losses and instrumental effects are included in calculating the reconstruction efficiency. The 4-lepton mass is required to be within $\pm 2\sigma_{4l}$ around m_{4l}. Significance for 10^4 pb^{-1}, calculated according to Poisson statistics, is also given in the table. With

10^4 pb^{-1}, the 5σ significance level is not reached for any value of m_H.

Figure 9 shows the signal significance versus m_H for different luminosities. With an integrated luminosity of 2×10^4 pb^{-1}, the Higgs mass reach at a 5σ significance level is from about 190 to about 350 GeV, and a first hint at 3σ significance could be obtained for $m_H \approx 190$ to 450 GeV. The significance is somewhat reduced around 300 GeV, due to the suppresed cross–section for $gg \to$ H for $m_{top} = 174$ GeV.

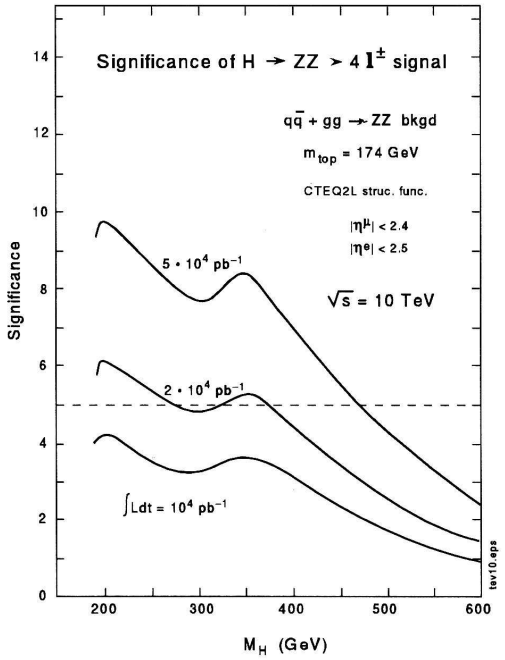

Fig. 9. Significance for H $\to$ ZZ $\to 4\ell^{\pm}$ *as a function of* m_H *for several* L_{int} *values at* $\sqrt{s} = 10$ TeV.

7. *Conclusion*

We have studied the detection possibilities for the Standard Model H $\to$ ZZ $\to 4\ell^{\pm}$ signal in the CMS detector at the nominal LHC energy $\sqrt{s} = 14$ TeV and at the reduced LHC energy $\sqrt{s} = 10$ TeV, including a detailed description of instrumental effects for both muons and electrons. Radiation losses for electrons are partly recovered by measuring electron energies in the crystal calorimeter, insuring a better Z mass reconstruction efficiency. The typical Z mass reconstruction efficiency in the Higgs mass range from $2m_Z$ threshold upwards is about 80%. Typical Z mass resolutions are $\sigma_Z \approx 1.8$ GeV for Z $\to \mu^+\mu^-$ for $m_H = 300$ GeV, and $\sigma_Z \approx 2.1$ GeV for Z $\to e^+e^-$. The 4-lepton resolutions are $\sigma_{4\mu} \approx 1.0$ GeV and $\sigma_{4e} \approx 2.0$ GeV for $m_H < 200$ GeV.

At the nominal LHC energy $\sqrt{s} = 14$ TeV and an integrated luminosity of 10^4 pb^{-1}, the Higgs mass reach at a 5σ significance level is found to be from about 190 to about 400 GeV, extending up to about 650 GeV at 10^5 pb^{-1}. The staging scenario with a crystal calorimeter limited to the barrel would result in a nonnegligible reduction of the signal significance.

The reduction of the LHC cms energy from 14 TeV to 10 TeV in the early phase of LHC operation leads to a significant degradation of signal significance, mainly due to the rapid fall of the production cross–section. With an integrated luminosity of 2×10^4 pb^{-1}, the H mass reach at a 5σ significance level is found to be from about 190 to about 350 GeV. In the mass range from about 250 to about 350 GeV, the calculated significance is close to 5σ and the about $\pm 15\%$ uncertainty on structure functions, and a more conservative assumption on the lepton reconstruction efficiency, would make it easily fall below the 5σ level.

References

1) CMS Technical Proposal, CERN/LHCC 94-38, 15 Dec. 1994;

2) T. Sjöstrand, PYTHIA 5.7 and JETSET 7.4 Physics and Manual, CERN-TH.7112/93, 1993;

3) F. Abe et al., CDF Collaboration, Phys. Rev. D **50** (1994) 2966;

4) E. W. N. Glover and J. J. van der Bij, Nucl. Phys. B **321** (1989) 561;

5) E. Barberio, B. van Eijk and Z. Was, Comp. Phys. Comm. **66** (1991) 115;

6) V. Karimäki, *Fast Tracker Response Simulation*, CMS TN/94-275 1994.; *Overall Muon Momentum Fit in the CMS Detector*, CMS T N/94-151, 1994.; *Muon Resolution in the CMS Detector*, CMS TN/92-12, 1992; V. Karimäki, M. Pimiä and G. Wrochna, *Optimization of Muon Momentum Measurement*, CMS TN/93-62, 1993.

7) I. Evangelou, *CMS Simulations for LHC, Electrons in Staging Scenarios*, CMS TN/93-68, 1993; *E/M Calorimeter Calibration with Electrons*, CMS-TN/92-07, 1992;

8) A. Nikitenko, P. Verrechia and D. Bomeštar, *I.* $Z \to e^+e^-$ *and* $H \to 4e^{\pm}$ *Mass Reconstruction with Full GEANT Simulation of CMS detector, II.Electrons of* $E_T = 30$ *GeV at* $\eta = 0.1$ *and 1.3 in CMS Detector: E/p Matching, Ca Libration, Resolution*, CMS TN/95-019, 1995;

9) I. Iashvili, R. Kinnunen and A. Nikitenko, *Study of* $H \to ZZ^* \to 4\ell^{\pm}$ *in CMS*, CMS TN/94-310, 1994 Berlin, 1966.

PROUČAVANJE $H \to ZZ \to 4\ell^{\pm}$ POMOĆU CJELOVITE GEANT SIMULACIJE DETEKTORA CMS

Proučava se detekcija $H \to ZZ \to 4\ell^{\pm}$ procesa u detektoru CMS na nominalnoj energiji LHC $\sqrt{s} = 14$ TeV i moguńost ranijeg opažanja na manjoj energiji od 10 TeV. Studija uključuje instrumentalne efekte za elektrone i muone i njihov utjecaj na razlučivanje višeleptonskih masa.